Polymer Journal (2015) 47, 797–801

www.nature.com/pj

ORIGINAL ARTICLE

Thermosensitive polymer-coated $La_{0.73}Sr_{0.27}MnO_3$ nanoparticles: potential applications in cancer hyperthermia therapy and magnetically activated drug delivery systems

Meysam Soleymani[1], Mohammad Edrissi[1] and Ali Mohammad Alizadeh[2]

Thermosensitive polymer-coated $La_{0.73}Sr_{0.27}MnO_3$ (LSMO) nanoparticles with a core-shell structure were prepared as a heat-generating agent for magnetic hyperthermia therapy and magnetically activated drug delivery systems. The magnetic cores of LSMO nanoparticles with an average particle size of 54 nm were prepared using the citrate gel method. Then, the surface of the nanoparticles was successfully coated with poly(*N*-isopropylacrylamide-co-acrylamide) (PNIPAAm-co-AAm) through admicellar polymerization method. First, the surfaces of the nanoparticles were coated with a bilayer surfactant containing oleic acid and SDS as an inner and outer layer surfactant, respectively. Then, the polymerization was carried out at 70 °C to enforce the adsolubilization of monomers in the hydrophobic interlayer between the two self-organized surfactants that coated each particle. The heat generation efficiency of the PNIPAAm-co-AAm-coated LSMO nanoparticles under various alternating magnetic fields was determined by induction heating analysis. The results showed that the maximum temperature attained by the nanoparticles falls within the desired therapeutic temperature range, which is suitable for cancer hyperthermia therapy and magnetically activated drug delivery systems.
Polymer Journal (2015) **47,** 797–801; doi:10.1038/pj.2015.66; published online 9 September 2015

INTRODUCTION

In recent years, significant attention has been paid to the application of magnetic nanoparticles (MNPs) in biomedicine and bioengineering, including magnetically activated drug delivery,[1] bio-separation,[2,3] magnetic resonance imaging,[4] biomacromolecule purification[5] and magnetic hyperthermia cancer therapy.[6,7] The concept of magnetic hyperthermia cancer therapy was first established by Gilchrist *et al.* in 1957.[8] This method involves introducing fluid-containing MNPs into a tumor and then subjecting the tumor tissue to an alternating magnetic field, leading to heat generation by the nanoparticles, which can destroy the tumors. However, the Curie temperature (T_c) of the most common magnetic materials used in biomedical fields, such as Fe_3O_4 ($T_c \approx 585\,^{\circ}C$) and γ-Fe_2O_3 ($T_c \approx 447\,^{\circ}C$), is higher than the desired temperature range, leading to damage to the surrounding healthy cells. As such, magnetic materials with a low T_c are preferred. $La_{1-x}Sr_xMnO_3$ perovskite oxides, with a tunable T_c in the body temperature range of $0.2 \leqslant x \leqslant 0.3$, are of particular interest for biomedical applications.[9]

However, bare MNPs are not sufficiently stable in physiological media. Consequently, the nanoparticle surface should be coated with a biocompatible shell to avoid aggregation and confer biocompatibility to the MNPs.[10] In addition, in magnetically activated drug delivery systems, MNPs are typically coated with a thermosensitive polymer to act as a drug carrier. When these nanoparticles are exposed to an alternating magnetic field, due to the heat generated by the magnetic core, the thermosensitive polymer undergoes a phase transition and the drug is released.[11,12] In addition, Yavuz *et al.*[13] have presented a platform based on Au nanocages coated with thermosensitive polymers for controlled drug release. When the Au nanocage is exposed to near-infrared light, heat is generated through the photothermal effect.[14] The heat will then dissipate into the surroundings and raise the temperature of the polymers, leading to chain collapse. Consequently, the pores of the nanocage open and the pre-loaded drug is finally released. A similar behavior has been reported for Au nanoparticles coated with a thermosensitive hydrogel.[15]

Currently, thermosensitive polymers, particularly those based on poly(N-isopropylacrylamide) (PNIPAAm) have attracted considerable attention in biomedical applications. PNIPAAm exhibits a phase transition at ~32 °C, called the lower critical solution temperature. At this temperature, a reversible hydration–dehydration of the amide groups occurs within the PNIPAAm chains.[16] At temperatures lower than the lower critical solution temperature, the polymer is

[1]Department of Chemical Engineering, Amirkabir University of Technology, Tehran, Iran and [2]Cancer Research Center, Tehran University of Medical Sciences, Tehran, Iran
Correspondence: Professor M Edrissi, Department of Chemical Engineering, Amirkabir University of Technology, Hafez Ave., Tehran 15875-4413, Iran.
E-mail: edrisi@aut.ac.ir
and Dr AM Alizadeh, Cancer Research Center, Tehran University of Medical Sciences, Keshavarz Ave., 14197-33141, Tehran, Iran.
E-mail: aalizadeh@sina.tums.ac.ir
Received 31 May 2015; revised 1 July 2015; accepted 9 July 2015; published online 9 September 2015

hydrophilic and completely soluble in aqueous media, but at higher temperatures it becomes hydrophobic. It has been found that the lower critical solution temperature of PNIPAAm can be tuned by the addition of appropriate hydrophilic monomers such as acrylamide (AAm) or acrylic acid (AA).[17,18] To date, only a limited number of studies have been published on coating MNPs with thermosensitive PNIPAAm derivatives. In this work, we coated $La_{0.73}Sr_{0.27}MnO_3$ (LSMO) nanoparticles with thermosensitive PNIPAAm-co-AAm copolymer via a admicellar polymerization route. To this end, a two-step synthetic method was performed: first, LSMO nanoparticles were coated with a bilayer surfactant; second, PNIPAAm and AAm chains were polymerized in the interlayer formed between the two surfactants surrounding each particle. The obtained products were characterized by means of X-ray diffraction analysis, Fourier transform infrared spectroscopy (FTIR), thermogravimetric analysis (TG) and transmission electron microscopy. In addition, the heating efficacy of the polymer-coated nanoparticles was evaluated by induction heating analysis.

MATERIALS AND METHODS

Materials

$La(NO_3)_3.6H_2O$, *N*-isopropylacrylamide (NIPAAm), AAm, ammonium persulfate, *N*,*N*,*N*′,*N*′-tetramethyl ethylene diamine (TEMED), *N*,*N*′-methylenebisacrylamide (BIS) were commercially obtained from Sigma-Aldrich Corp., St Louis, MO, USA, and used without further purification. $Mn(NO_3)_2.4H_2O$, $Sr(NO_3)_3$, citric acid ($C_6H_8O_7$), ethylene glycol, oleic acid (OA), SDS and ammonia solution (NH_4OH, 25 wt%) were purchased from Merck, Darmstadt, Germany, and used without further purification.

Synthesis of LSMO nanoparticles

LSMO nanoparticles with a perovskite structure were prepared by the citrate gel method with a slight modification.[19,20] The metal nitrates of lanthanum, strontium and manganese were used as starting materials. Suitable proportions of these components were dissolved in deionized water to prepare 2 g of the LSMO nanoparticles. The obtained solution was mixed with citric acid and ethylene glycol to obtain the molar ratio of total metal/citric acid/ethylene glycol = 1/1.5/1.5. On heating this mixture on a hot plate at 75–80 °C, a viscous transparent gel was obtained. The gel was dried in an oven at 160 °C overnight to produce a solid amorphous precursor. The precursor was ground and then calcined at 800 °C for 4 h to obtain very light and black-colored flakes containing extremely fine particles.

Coating the LSMO nanoparticles with the thermosensitive polymer

To encapsulate the LSMO nanoparticles with the thermosensitive polymer, the surfaces of the nanoparticles were coated with a bilayer surfactant containing OA and SDS as the inner and outer layer, respectively. To this end, 60 mg of the LSMO nanoparticles dispersed in 50 ml of deionized water were vigorously mixed with 0.2 ml of OA at 75–80 °C. After 1 h, the flocculated nanoparticles were easily separated and washed several times with hot water to remove unreacted OA. Then, 0.02 g of SDS dispersed in 50 ml of deionized water was added to the solution containing the OA-coated nanoparticles and sonicated for 15 min to obtain the self-organized bilayer surfactant on the surface of the nanoparticles. The coated nanoparticles were then isolated by magnetic decantation, and they were washed several times with deionized water and ethanol to remove the residual surfactant.

The surface-modified LSMO nanoparticles were then coated with poly (N-isopropylacrylamide-co-acrylamide) (PNIPAAm-co-AAm) through an admicellar polymerization reaction.[21] To achieve this, 0.15 g of NIPAAm, 0.018 g of AAm and 0.013 g of BIS were dissolved in 30 ml of deionized water. The surface-modified LSMO nanoparticles were then added to the mixture. The solution was heated at 70 °C with vigorous stirring under a nitrogen atmosphere. Subsequently, 0.007 g of ammonium persulfate and 100 μl of TEMED were added to the solution and stirred for 6 h. Finally, the obtained nanoparticles were separated by centrifugation and washed several times with deionized water.

Characterization of nanoparticles

The crystalline structure of the samples was determined by X-ray diffraction analysis at room temperature using a Philips X'Pert powder diffractometer (Amsterdam, Netherlands) with CuKα radiation and a Ni filter ($\lambda = 0.15418$ nm). Transmission electron microscope (Zeiss-EM10C-80 KV, Oberkochen, Germany) was used to determine the size and the shape of the synthesized nanoparticles. FTIR spectra were recorded in transmission mode using a JASCO FTIR 680-Plus spectrometer (Tokyo, Japan) in the region of 400–4000 cm^{-1}. TG analysis was performed using a Perkin-Elmer Diamond TG/DTA instrument (Waltham, MA, USA).

Induction heating analysis

The heating efficacy of the surface-modified silica-coated LSMO nanoparticles was evaluated using a custom-made induction heating unit with a five turns (5 cm diameter) induction coil. An aqueous suspension of the PNIPAAm-co-AAm at LSMO nanoparticles (1.5 ml) was placed in the center of the induction coil and then irradiated by different magnetic fields ($H = 6$, 10 and 12 $kA\,m^{-1}$, and $f = 100$ kHz). The temperature of the sample was monitored by an alcohol thermometer. To evaluate the heat generation efficacy of the nanoparticles, the specific absorption rate of the sample was calculated according to Equation (1):

$$SAR = \left(\frac{C_{suspension}}{X_{NP}}\right)\left(\frac{dT}{dt}\right) \quad (1)$$

where $C_{suspension}$ is the specific heat of the suspension ($C_{water} \approx 4.18\,J\,g^{-1}\,k^{-1}$ and $C_{NP} \approx 0.66\,J\,g^{-1}\,k^{-1}$],[22] X_{NP} is the weight fraction of nanoparticles ($X_{NP} =$ 0.03, 0.05 and 0.10) and dT/dt is the initial slope of the temperature curve versus time.

RESULTS AND DISCUSSION

The polymerization of organic monomers on the surface of organic particles easily occurs. However, when the polymerization occurs in the presence of inorganic particles, seed nucleation and growth of the organic monomers is found to occur independent of the inorganic particles.[21] Therefore, it is necessary to modify the surface of inorganic particles to improve the affinity between the particles and the monomers. In this study, the MNPs were coated with a bilayer surfactant to create a hydrophobic region inside the bilayer in close vicinity to the particles, which can be used to polymerize the hydrophobic monomers close to the particle surface to form a core-shell nanostructure (Figure 1). In addition, coating MNPs with a bilayer surfactant increases the stability and dispersibility of the particles in aqueous media. The process that was used to prepare the bilayer surfactant on the surface of the LSMO nanoparticles is as follows: first, OA was used to modify the surface of the particles. OA has a high affinity to the LSMO nanoparticle surface and thus forms a hydrophobic layer on the surface of the particles, leading to the flocculation of the nanoparticles in aqueous media. The flocculation of the nanoparticles confirms the formation of a single OA layer on the surface of the nanoparticles. To prepare water-dispersible LSMO nanoparticles, the obtained particles were coated with SDS as a secondary surfactant to form the self-organized double-layer surfactant on the surface of the nanoparticles (Figure 1).

X-ray diffraction analysis

Figure 2 shows the crystalline structure of bare (curve a) and PNIPAAm-co-AAm@LSMO nanoparticles (curve b). In curve a, the observed diffraction peaks with a 2θ at 22.9, 32.7, 40.3, 46.9, 53.1, 58.3 and 68.6° indicate the cubic perovskite structure of the LSMO nanoparticles.[23] The same set of characteristic peaks was also observed for polymer-coated LSMO nanoparticles, indicating the crystalline

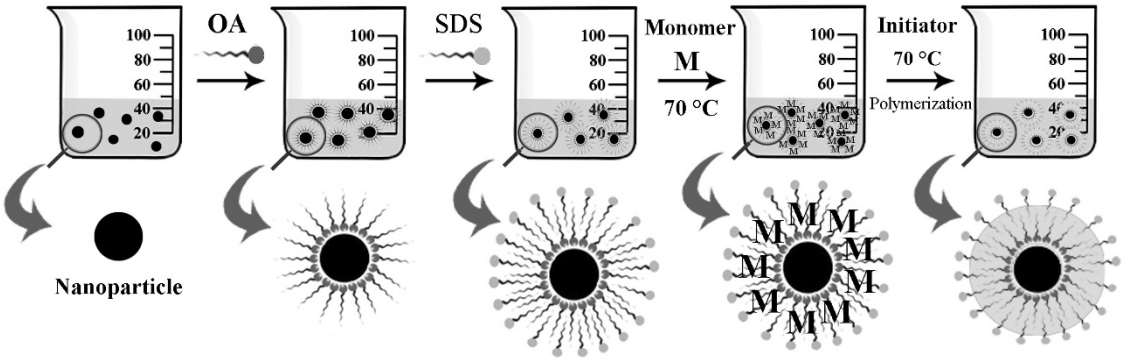

Figure 1 Schematic representation of bilayer surfactant-coated LSMO nanoparticles and the polymerization of PNIPAAm-co-AAm on the surface of the nanoparticles. LSMO, $La_{0.73}Sr_{0.27}MnO_3$; PNIPAAm-co-AAm, poly(*N*-isopropylacrylamide-co-acrylamide. A full color version of this figure is available at *Polymer Journal* online.

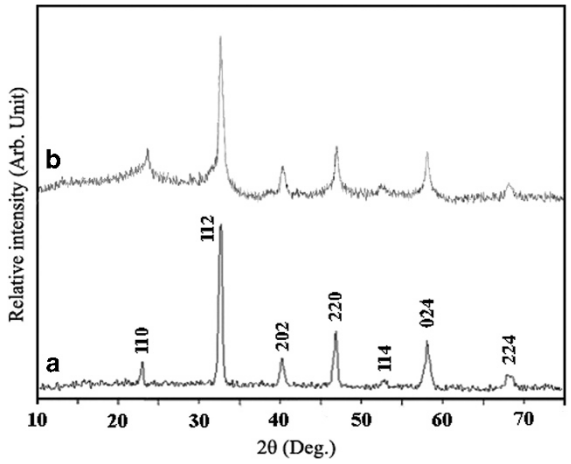

Figure 2 XRD patterns of (**a**) bare and (**b**) PNIPAAm-co-AAm at LSMO nanoparticles. LSMO, $La_{0.73}Sr_{0.27}MnO_3$; PNIPAAm-co-AAm, poly(*N*-isopropylacrylamide-co-acrylamide; XRD, X-ray diffraction.

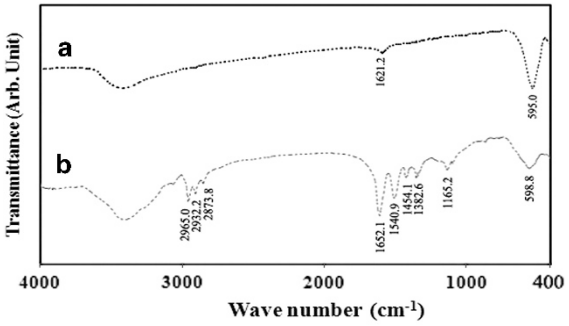

Figure 3 FTIR spectra of (**a**) bare and (**b**) PNIPAAm-co-AAm at LSMO nanoparticles. FTIR, Fourier transform infrared spectroscopy; LSMO, $La_{0.73}Sr_{0.27}MnO_3$; PNIPAAm-co-AAm, poly(*N*-isopropylacrylamide-co-acrylamide.

phase of the LSMO nanoparticles does not change during the polymer coating process. In addition, when the LSMO nanoparticles are coated with the thermosensitive polymer, a hump at $\sim 2\theta = 24°$ is observed, which confirms the existence of the amorphous PNIPAAm-co-AAm shell on the surface of the LSMO nanoparticles.

FTIR analysis

The crystalline structure of the LSMO perovskite oxides is similar to the distorted $GdFeO_3$-type structure in which a central Mn cation is surrounded by six oxygen anions in an octahedral arrangement. The MnO_6 has a nearly ideal octahedral symmetry with six vibrational modes; however, only two of them are activated using infrared irradiation.[19] The band at $\sim 600\,cm^{-1}$ is related to the stretching mode (ν_s) of the Mn–O or Mn–O–Mn bonds, and the band at $\sim 400\,cm^{-1}$ corresponds to the bending mode (ν_b) of the Mn–O–Mn bond, which is due to the change in the bond angle.[24]

The FTIR spectra of the bare (curve a) and polymer-coated LSMO nanoparticles (curve b) are shown in Figures 3a and b, respectively. In curve a, absorption bands at ~ 595 and $400\,cm^{-1}$ are observed, which correspond to the stretching and bending modes of the Mn–O–Mn bond, respectively. The appearance of these bands in the FTIR spectrum of the bare nanoparticles suggests that the LSMO nanoparticles with a perovskite structure have been formed at 800 °C, which is in agreement with the X-ray diffraction results. The absorption bands at 1621.2 and $3427.0\,cm^{-1}$ are due to the stretching and bending modes of H–O–H, free or adsorbed water on the surface of nanoparticles, respectively. To confirm the presence of the polymer shell on the surface of the LSMO nanoparticles after coating process was carried out, FTIR analysis was performed on the obtained sample and the result is shown in Figure 3b. Compared with the bare LSMO nanoparticles, several new absorption peaks are observed in the FTIR spectrum of the coated particles. The absorption bands at 1652.1, 1540.9 and $1454.1\,cm^{-1}$ are assigned to the stretching vibrations of a C = O and the bending vibration of an –NH and $–NH_2$ group, respectively. The band that appears at $1382.6\,cm^{-1}$ corresponds to the bending vibrations of the isopropyl C–H groups. The absorption peaks at 2873.8, 2932.2 and $2965.0\,cm^{-1}$ are assigned to the asymmetric and symmetric stretching vibrations of the C–H groups. The absorption band that appears at $\sim 3450\,cm^{-1}$ is related to the stretching vibration of the –NH groups from NIPAAm and AAm. The characteristic absorption band of the LSMO nanoparticles was also observed at $598.8\,cm^{-1}$ in the spectrum of the polymer-coated LSMO nanoparticles, with a smaller intensity because the surface of the nanoparticles is shielded by the polymer shell coating.

TG analysis

TG measurements of the bare (curve a) and PNIPAAm-co-AAm at LSMO nanoparticles (curve b) are shown in Figure 4. The bare LSMO

nanoparticles (curve a) show a small weight loss of ~1.2% over the entire temperature range tested, which can be attributed to the evaporation of adsorbed water from the surface of nanoparticles. For the polymer-coated LSMO nanoparticles, a total weight loss of ~38.5% is observed, which is predominantly due to the evaporation of adsorbed water and the thermal decomposition of OA, SDS and the polymer coating. This result indicates that the LSMO nanoparticles accounts for ~61.5% of the final product from the calculated mass according to TG results.

Transmission electron microscopic analysis

The transmission electron microscopy image and corresponding particle size distribution of the bare LSMO nanoparticles are shown in Figure 5a. Figure 5a shows that the bare LSMO nanoparticles have an irregular shape with an average particle size of 54 nm. In Figure 5b, the formation of a core-shell structure can be confirmed by two distinguishable regions with different electron densities. The high electron density (darker) region corresponds to the LSMO nanoparticles, whereas the transparent or low electron density region surrounding the core corresponds to the polymer shell that coats the nanoparticles with a thickness of approximately 6 nm.

Induction heating analysis

A home-made induction heating unit was used to produce the desired alternating magnetic field. The frequency and the intensity of the applied magnetic field in all experiments was 100 kHz and 10 kA m^{-1}, which are within the safe range for use in biomedical applications.[25]

The time-dependent temperature curves for the aqueous suspensions of PNIPAAm-co-AAm at LSMO nanoparticles (30, 50 and 100 mg ml^{-1}) exposed to an alternating magnetic field are shown in Figure 6. As can be observed, by applying a magnetic field, the temperature of the magnetic fluids increased and saturated at 47, 49.5 and 56.3 °C at particle concentrations of 30, 50 and 100 mg ml^{-1}, respectively. This saturation arises due to the equilibrium between the heat generated from the nanoparticles and the heat dissipated to the

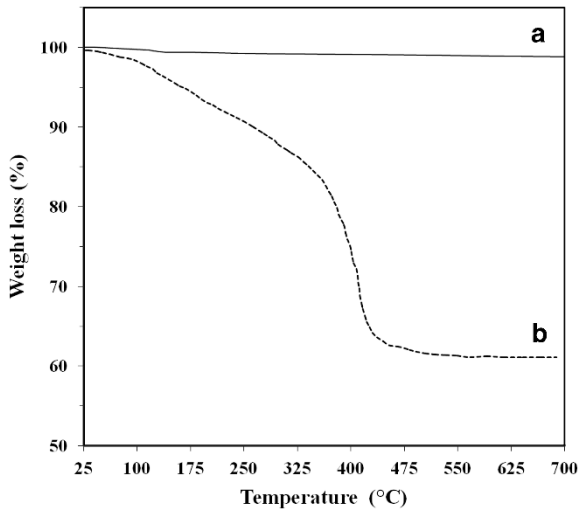

Figure 4 Thermogravimetric analysis of (**a**) bare and (**b**) polymer-coated LSMO nanoparticles. LSMO, $La_{0.73}Sr_{0.27}MnO_3$.

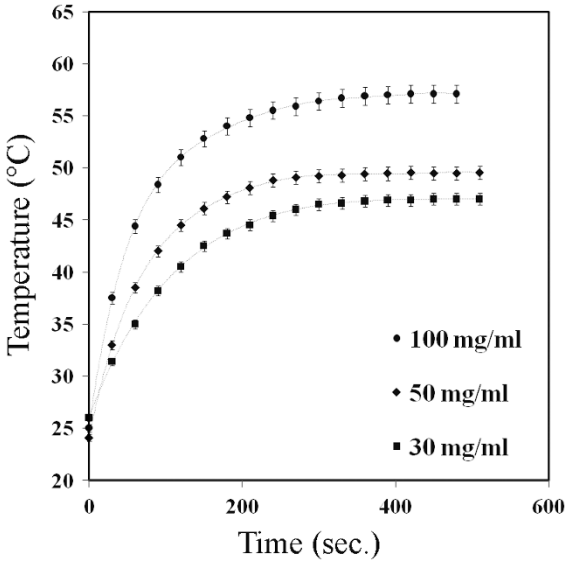

Figure 6 Temperature versus time for aqueous suspensions of PNIPAAm-co-AAm at LSMO nanoparticles at different concentrations. LSMO, $La_{0.73}Sr_{0.27}MnO_3$; PNIPAAm-co-AAm, poly(*N*-isopropylacrylamide-co-acrylamide.

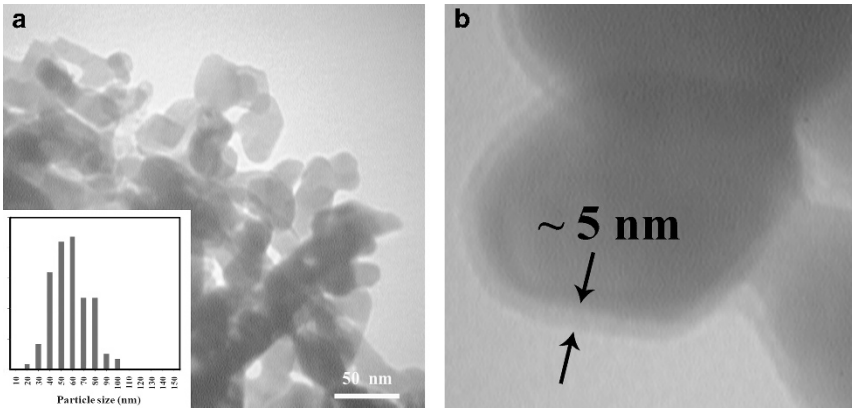

Figure 5 TEM images of (**a**) bare (inset shows particle size distribution) and (**b**) polymer-coated LSMO nanoparticles. LSMO, $La_{0.73}Sr_{0.27}MnO_3$; TEM, transmission electron microscopy. A full color version of this figure is available at *Polymer Journal* online.

surroundings, and also a decrease of the magnetization due to approaching the T_c.

In addition, the final temperature of all samples falls within the desired temperature range, which suggests that these thermosensitive polymer-coated LSMO nanoparticles can safely produce the required heat for magnetic hyperthermia or magnetically activated drug delivery systems in response to a safe alternating magnetic field. In addition, the specific absorption rate values of the magnetic fluids at different nanoparticle concentrations were measured through the initial slope of the heating curves. The obtained SAR values were 27.3, 28.8 and 20.1 W per g_{NP} for particle concentrations of 30, 50 and 100 mg ml^{-1}, respectively.

CONCLUSIONS

Magnetic LSMO nanoparticles with an average particle size of 54 nm were prepared by the citrate gel method. The obtained LSMO nanoparticles were then successfully encapsulated with a thermosensitive copolymer PNIPAAm-co-AAm shell through admicellar polymerization. To this end, the surface of the nanoparticles was coated with a bilayer surfactant containing OA and SDS as an inner and outer layer surfactant, respectively. Then, the polymerization was carried out at 70 °C to enforce the adsolubilization of the monomers in the hydrophobic interlayer between the two self-organized surfactants coating each particle. The heating efficacy of the PNIPAAm-co-AAm at LSMO nanoparticles was evaluated under different alternating magnetic fields ($H = 6$, 10 and 12, $f = 100$ kHz). The results showed that the maximum temperature attained by the nanoparticles falls within the desired therapeutic temperature range (45–60 °C), which is suitable for biomedical applications.

CONFLICT OF INTEREST

The authors declare no conflict of interest.

ACKNOWLEDGEMENTS

This study was supported by a grant from the Tehran University of Medical Sciences (Grant Number: 27707).

1 Mc Bain, S. C., Yiu, H. H. & Dobson, J. Magnetic nanoparticles for gene and drug delivery. *Int. J. Nanomed.* **3**, 169–180 (2008).
2 Tibbe, A. G. J., de Grooth, B., Greve, J., Liberti, P. A., Dolan, G. J. & Terstappen, L. W. M. M. Optical tracking and detection of immunomagnetically selected and aligned cells. *Nat. Biotechnol.* **17**, 1210–1213 (1999).
3 Liberti, P. A., Rao, C. G. & Terstappen, L. W. M. M. Optimisation of ferrofluids and protocols for the enrichment of breast tumor cells in blood. *J. Magn. Magn. Mater.* **225**, 301–307 (2001).
4 Zhang, M., Jugold, E., Woenne, T., Lammers, B., Morgenstern, M. M., Mueller, H., Zentgraf, M., Bock, M., Eisenhut, W., Semmler & Kiessling, F. Specific targeting of tumor angiogenesis by RGD-conjugated ultra-small superparamagnetic Iron oxide particles using a clinical 1.5-T magnetic resonance scanner. *Cancer Res.* **67**, 1555–1562 (2007).
5 Elaissari, A., Rodrigue, M., Meunier, F. & Herve, C. Hydrophilic magnetic latex for nucleic acid extraction, purification and concentration. *J. Magn. Magn. Mater.* **225**, 127–133 (2001).
6 Jordan, A., Scholz, R., Wust, P., Fahling, H. & Felix, R. Magnetic fluid hyperthermia (MFH): cancer treatment with AC magnetic field induced excitation of biocompatible superparamagnetic nanoparticles. *J. Magn. Magn. Mater.* **201**, 413–419 (1999).
7 Jordan, A., Scholz, R., Wust, P., Schirra, H., Schiestel, T., Schmidt, H. & Felix, R. Endocytosis of dextran and silan-coated magnetite nanoparticles and the effect of intracellular hyperthermia on human mammary carcinoma cells in vitro. *J. Magn. Magn. Mater.* **194**, 185–196 (1999).
8 Gilchrist, R. K., Medal, R., Shorey, W. D., Hanselman, R. C., Parrott, J. C. & Taylor, C. B. Selective inductive heating of lymph nodes. *Ann. Surg.* **146**, 596–606 (1957).
9 Asamitsu, A., Morimoto, Y., Kumai, R., Tomioka, Y. & Tokura, Y. Magnetostructural phase transitions in $La_{1-x}Sr_xMnO_3$ with controlled carrier density. *Phys. Rev. B* **54**, 1716–1723 (1996).
10 Vonarbourg, A., Passirani, C., Saulnier, P. & Benoit, J. P. Parameters influencing the stealthiness of colloidal drug delivery systems. *Biomaterials* **27**, 4356–4373 (2006).
11 Kumar, S. S. R. & Mohammad, C. F. Magnetic nanomaterials for hyperthermia-based therapy and controlled drug delivery. *Adv. Drug Deliv. Rev.* **63**, 789–808 (2011).
12 Li, J., Qu, Y., Ren, J., Yuan, W. & Shi, D. Magnetocaloric effect in magnetothermally-responsive nanocarriers for hyperthermia-triggered drug release. *Nanotechnology* **23**, 505706 (2012).
13 Yavuz, M. S., Cheng, Y., Chen, J., Cobley, C. M., Zhang, Q., Rycenga, M., Xie, J., Kim, C., Song, K. H., Schwartz, A. G., Wang, L. V. & Xia, Y. Gold nanocages covered by smart polymers for controlled release with near-infrared light. *Nat. Mater.* **8**, 935–939 (2009).
14 Liu, G. L., Kim, J., Lu, Y. & Lee, L. P. Optofluidic control using photothermal nanoparticles. *Nat. Mater.* **5**, 27–32 (2005).
15 Kim, J. H. & Lee, T. R. Thermo- and pH-responsive hydrogel-coated gold nanoparticles. *Chem. Mater.* **16**, 3647–3651 (2004).
16 Yoshida, R., Uchida, K., Kaneko, Y., Sakai, K., Kikuchi, A., Sakurai, Y. & Okano, T. Comb-type grafted hydrogels with rapid deswelling response to temperature changes. *Nat* **374**, 240–242 (1995).
17 Kayi, H., Tuncel, S. A., Elkamel, A. & Alper, E. Prediction of lower critical solution temperature of N-isopropylacrylamide-acrylic acid copolymer by an artificial neural network model. *J. Mol. Model.* **11**, 55–60 (2005).
18 Mai, T. T. T., Le, T. H. P., Pham, H. N., Do, H. M. & Nguyen, X. P. Synthesis and magnetic heating characteristics of thermoresponsive poly (N-isopropylacrylamide-co-acrylic acid)/nano Fe_3O_4 nanparticles. *Adv. Nat. Sci. Nanosci. Nanotechnol.* **5**, 045007 (2014).
19 Soleymani, M., Moheb, A. & Joudaki, E. High surface area nano-sized La0.6Ca0.4MnO3 perovskite powder prepared by low temperature pyrolysis of a modified citrate gel. *Cent. Eur. J. Chem.* **7**, 809–817 (2009).
20 Soleymani, M., Moheb, A. & Babakhani, D. Hydrogen peroxide decomposition over nanosized $La_{1-X}Ca_XMnO_3$ ($0 \leq X \leq 0.6$) perovskite oxides. *Chem. Eng. Technol.* **34**, 49–55 (2011).
21 Meguro, K., Yabe, T., Ishioka, S., Kato, K. & Esumi, K. Polymerization of styrene adsolubilized in surfactant adsorbed bilayer on pigments. *Bull. Chem. Soc. Jpn* **59**, 3019–3021 (1986).
22 Kim, D., Zink, B. L., Hellman, F. & Coey, J. M. D. Critical behavior of $La_{0.75}Sr_{0.25}MnO_3$. *Phys. Rev. B* **65**, 214424 (2002).
23 Sayagues, M. J., Cordoba, J. M. & Gotor, F. J. Room temperature mechanosynthesis of the $La_{1-x}Sr_xMnO_{3\pm\delta}$ ($0 \leq x \leq 1$) system and microstructural study. *J. Solid State Chem.* **188**, 11–16 (2012).
24 Wang, X., Cui, Q., Pan, Y. & Zou, G. X-Ray photoelectron and infrared transmission spectra of manganite system $La_{0.5-x}Bi_xCa_{0.5}MnO_3$ ($0 \leq x \leq 0.25$). *J. Alloys Compd.* **354**, 91–94 (2003).
25 Minamimura, T., Sato, H., Kasaoka, S., Saito, T., Ishizawa, S., Takemori, S., Tazawa, K. & Tsukada, K. Tumor regression by inductive hyperthermia combined with hepatic embolization using dextran magnetite-incorporated microspheres in rats. *Int. J. Oncol.* **16**, 1153–1158 (2000).